Int. J. Heat Mass Transfer. Vol. 21, pp. 25–33. Pergamon Press 1978. Printed in Great Britain

LAMINAR JET IMPINGEMENT HEAT TRANSFER INCLUDING THE EFFECTS OF MELTING

A. W. LIPSETT* and R. R. GILPIN†
Department of Mechanical Engineering, University of Alberta,
Edmonton, Alberta, Canada

(*Received* 3 *November* 1976 *and in revised form* 17 *March* 1977)

Abstract—The problem of the heat transfer from a laminar water jet to the surface on which it impinges is studied analytically. The jet flow is divided into two parts, a potential flow region and a boundary-layer region. The solution of the potential flow problem is obtained using a finite element method. The boundary-layer problem is solved by a Karman–Pohlhausen integral method.

This method of treating jet impingement heat-transfer problems is tested for two-dimensional planar and axisymmetric flows. Results are also presented which include the effects of melting occurring at the impingement surface.

NOMENCLATURE

e, element number;
h, distance between nozzle exit and impingement surface;
m, ratio of thermal to momentum boundary-layer thicknesses;
m_0, ratio of boundary-layer thicknesses at stagnation point;
n, indicator for geometry (1 = axisymmetric and 0 = planar two-dimensional);
q_L, latent heat of fusion;
$r(x)$, function defining impingement surface;
s, distance along impingement surface;
u, boundary-layer velocity along impingement surface;
v, boundary-layer velocity perpendicular to the impingement surface;
v_n, potential flow velocity normal to the boundary;
v_0, fluid injection velocity due to melting;
v_R, v_Z, v_X, v_Y, velocity components in potential flow region;
x, y, coordinates in boundary layer parallel and perpendicular to impingement surface;
A^e, area of element e;
C_p, specific heat of water;
D, diameter of axisymmetric jet or jet width in two-dimensional case;
H, normalized nozzle-plate spacing, h/D;
I, integral to be minimized;
K, transformed dependent variable, $\delta_2^2 \dfrac{dU}{dx}$;
L, transformed variable, $\delta_3^2 \dfrac{dU}{dx}$;
Nu_D, Nusselt number based on D;
Pr, Prandtl number;
R, Z, axisymmetric coordinates in potential flow;
Re_D, Reynolds number based on D;
S_{ij}, stiffness matrix in two-dimensional case;
SA_{ij}, stiffness matrix in axisymmetric case;
SL_i, load matrix in two-dimensional case;
SLA_i, load matrix in axisymmetric case;
Ste, Stefan number;
T_0, temperature of impingement surface (for melting 0°C);
T_∞, bulk fluid temperature;
U, free stream velocity along impingement surface;
U_f, free surface velocity;
V, jet velocity;
W, variable δ_3^2;
X, Y, two-dimensional coordinates in potential flow region;
Z, variable δ_2^2.

Greek symbols

δ_1, displacement thickness;
δ_2, momentum thickness;
δ_3, energy thickness;
δ_u, momentum boundary-layer thickness;
δ_t, thermal boundary-layer thickness;
η, nondimensional distance in boundary layer, y/δ_t;
η_1, nondimensional distance in boundary layer, y/δ_u;
λ_0, melting parameter, $v_0\delta_t/6$;
λ_0', melting parameter, $v_0\delta_u/6$;
ξ_i, area coordinate;
ϕ, velocity potential;
ϕ^*, specified potential on boundary;
Δ_1, ratio δ_1/δ_u;
Δ_2, ratio δ_2/δ_u;
Δ_3, ratio δ_3/δ_t;

*Graduate student.
†Associate Professor of Mechanical Engineering.

θ, nondimensional temperature $(T-T_0)/(T_\infty-T_0)$;
Λ, pressure gradient parameter, $\delta_u^2\,\mathrm{d}U/\mathrm{d}x$;
Λ_0, parameter Λ at stagnation point.

INTRODUCTION

THE HEAT-TRANSFER process near a melting flat surface has been investigated by a number of authors [1–3]. These studies have dealt with the laminar boundary layer which grows on a flat surface in the absence of a pressure gradient. Pozvonkov, Shurgalskii and Akselrod [2] and Griffen [3] used the von-Karman–Pohlhausen integral method for their investigation. In order to study the effects of a water jet impinging on an ice surface the extension of the above works to include a pressure gradient is required. Gilpin [4] and Yen and Zehnder [5] have experimentally studied the heat-transfer characteristics associated with a water jet impinging on an ice surface. The use of jet impingement heat transfer for ice removal or for cutting ice may have applications wherever icing is a problem or the cutting of ice is required [6].

POTENTIAL FLOW PROBLEM FORMULATION AND SOLUTION

As with many forced convection fluid problems the division of this problem into a potential flow and a boundary layer is appropriate. For the solution of the potential flow the finite element method [7] is used. The finite element method offers a very flexible method of solution, being able to solve planar two-dimensional and rotationally symmetric (axisymmetric) potential flows equally well. Also boundaries of arbitrary shape are easily modeled by the finite element method. Sarpkaya and Hiriart [8] have used the finite element method to solve for the potential flow field of an axisymmetric jet impinging on curved thrust reversers. The following analysis follows that presented in [7] and is valid for either two-dimensional plane or axisymmetric incompressible, inviscid jet impinging on an arbitrarily shaped surface. A schematic of the flow field in non-dimensional form for an impinging jet is shown in Fig. 1. All distances are non-dimensionalized with respect to the jet diameter or jet slot-width D and all velocities non-dimensionalized with respect to the incoming jet velocity V. The coordinate directions for axisymmetric flow are R, Z and the governing equation for the flow in terms of the velocity potential ϕ is

$$\frac{\partial^2\phi}{\partial R^2}+\frac{1}{R}\frac{\partial\phi}{\partial R}+\frac{\partial^2\phi}{\partial Z^2}=0. \tag{1}$$

For two-dimensional planar flow the coordinate directions are X and Y and the governing equation for the flow is

$$\frac{\partial^2\phi}{\partial X^2}+\frac{\partial^2\phi}{\partial Y^2}=0. \tag{2}$$

The velocity potential ϕ is non-dimensionalized with respect to the incoming jet velocity V and the jet diameter or slot-width D. The formulation can just as

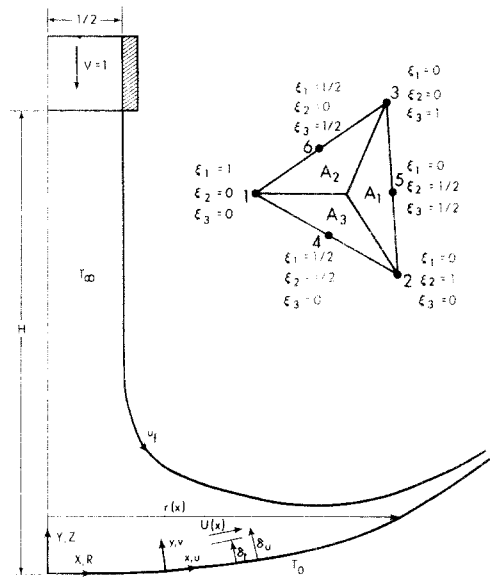

FIG. 1. Coordinate systems for the potential flow and boundary-layer regions and notation for a triangular element.

easily be made in terms of the streamfunction ψ. For axisymmetric flow the solution of Laplace's equation (1), satisfying specified normal velocity boundary conditions

$$v_n=\frac{\partial\phi}{\partial n}=V^* \quad \text{on the surface } \Gamma_1 \tag{3}$$

and specified potential boundary conditions

$$\phi=\phi^* \quad \text{on the surface } \Gamma_2 \tag{4}$$

is given by the function $\phi(R,Z)$ which minimizes the functional [7].

$$I(\phi)=\pi\iint_M\left|\left(\frac{\partial\phi}{\partial R}\right)^2+\left(\frac{\partial\phi}{\partial Z}\right)^2\right|R\,\mathrm{d}R\,\mathrm{d}Z - 2\pi\int_{\Gamma_1}\phi V^* R\,\mathrm{d}s \tag{5}$$

where M is the half-meridonal section of the flow and Γ_1 and Γ_2 make up the complete bounding curve of this area. In the case of two-dimensional flow the solution of equation (2) with boundary conditions (3) and (4) is given by the function $\phi(X,Y)$ which minimizes the functional

$$I(\phi)=\iint_M\left|\left(\frac{\partial\phi}{\partial X}\right)^2+\left(\frac{\partial\phi}{\partial Y}\right)^2\right|\mathrm{d}X\,\mathrm{d}Y - 2\int_{\Gamma_1}\phi V^*\,\mathrm{d}s \tag{6}$$

where M is now the half cross-section of the flow and Γ_1 and Γ_2 the complete bounding curve for this area.

The finite element method achieves an approximate minimization of the functional $I(\phi)$ by dividing the flow region into a set of E triangular elements and noting that

$$I(\phi)=\sum_{e=1}^{E}I^e(\phi^e) \tag{7}$$

where $I^e(\phi^e)$ is the functional (5) or (6) evaluated over the element e. A six-node triangular element with corner and midside nodes allows the variation of the velocity potential, ϕ^e within each element to be represented by a quadratic function of the velocity potential at each of the six nodes. In terms of the area coordinates $\xi_i = A_i/A^e$, $i = 1, 2, 3$ as shown in Fig. 1 leads to

$$\phi^e = \xi_1(2\xi_1 - 1)\phi_1^e + \xi_2(2\xi_2 - 1)\phi_2^e + \xi_3(2\xi_3 - 1)\phi_3^e + 4\xi_1\xi_2\phi_4^e + 4\xi_2\xi_3\phi_5^e + 4\xi_3\xi_1\phi_6^e. \quad (8)$$

The velocity components within each element are given by

$$v_R^e = \frac{\partial\phi^e}{\partial R}; \quad v_Z^e = \frac{\partial\phi^e}{\partial Z};$$

$$v_X^e = \frac{\partial\phi^e}{\partial X}; \quad v_Y^e = \frac{\partial\phi^e}{\partial Y}. \quad (9)$$

A linear transformation exists between the area coordinates ξ_i and coordinates R and Z, or X and Y. An obvious constraint on the area coordinates is

$$\xi_1 + \xi_2 + \xi_3 = 1. \quad (10)$$

Substitution of equations (8) and (9) into equation (5) for the eth element yields, using a Ritz technique,

$$\frac{\partial I^e(\phi^e)}{\partial\phi_i^e} = SA_{ij}\phi_j^e - SLA_i = 0. \quad (11)$$

The matrices SA_{ij} and SLA_i represent the element stiffness and load matrices for the axisymmetrical triangular element. For the two-dimensional case the minimization of equation (6) results in, for the *eth* element,

$$\frac{\partial I^e(\phi^e)}{\partial\phi_i^e} = S_{ij}\phi_j^e - SL_i = 0 \quad (12)$$

where S_{ij} and SL_i are the stiffness and load matrices for the two-dimensional element. Chan [9] has tabulated the matrices S_{ij}, SL_i, SA_{ij} and SLA_i which are determined once and for all because of the use of the area coordinates. An assembly procedure to include the effects of all of the elements results in a linear, symmetric and banded system of equations whose solution yields the velocity potential at each nodal point. The velocity at each of the nodal points is then obtained using equation (9).

A difficulty with this jet impingement flow is that a free surface is present and its position is not originally known and must be found as part of the solution. Therefore an iterative procedure is used to find the position of the free surface. First an initial guess as to its location is made and the finite element procedure employed to calculate the velocity at each node on the free surface. In the absence of gravity effects the boundary condition to be satisfied is that the free surface be a streamline of constant velocity. The position of each nodal point on the free surface was therefore adjusted in order to achieve this constant velocity condition. The adjustment procedure used is similar to that used by Sarpkaya and Hiriart [8] and is based qualitatively on the continuity requirements for the flow. At a node where the velocity exceeded the expected constant velocity the node was moved along an outward pointing normal to the local free surface a distance

$$\lambda\left|\left(\frac{U_f'}{U_f}\right)^2 - 1\right|.$$

Alternatively if the velocity was less than the expected value, the node was moved into the flow field by an amount given by the same expression. In this expression U_f' is the magnitude of the calculated nodal velocity, U_f is the expected magnitude and λ is a relaxation parameter which was chosen to ensure convergence. A value of $\lambda = 0.015$ was normally used. The calculation of the free surface velocity and the readjustment of its position was repeated until the constant velocity boundary condition was satisfied to within 1% at each node. The number of iterations required for convergence depends on the quality of the initial guess but typically 10–15 iterations were required.

The inputs required for the boundary-layer calculations to follow are the distributions of velocity and the gradient in velocity along the impingement surface. To obtain these parameters from the velocity potential calculated by the finite element scheme differentiations are, of course, required. The accuracy of these differentiations is critical in determining the accuracy of the heat-transfer results. First the velocity can be determined by an explicit differentiation of the potential function, equation (8), in each element. In this regard the use of the quadratic potential function was essential for minimizing the discontinuities in velocity occurring between adjacent elements. Next to obtain the gradient in velocity along the impingement surface a cubic spline [12] numerical differentiation of the element velocities was used. This scheme gave a smoothly varying approximation to the velocity gradient which could be used in the boundary-layer analysis.

BOUNDARY-LAYER PROBLEM FORMULATION AND SOLUTION

The jet impingement melting heat-transfer boundary-layer problem is formulated by considering the continuity equation and the momentum and thermal energy boundary-layer equations. The phase transformation is assumed to take place under steady-state conditions. All physical properties are assumed constant and viscous dissipation is neglected. Notation to be used for the boundary-layer analysis is shown in Fig. 1. Letting $n = 0$ correspond to two-dimensional planar flow and $n = 1$ correspond to axisymmteric flow the governing equations are in non-dimensional form

$$\frac{\partial(r^n u)}{\partial x} + \frac{\partial(r^n v)}{\partial y} = 0 \quad (13)$$

$$u\frac{\partial u}{\partial x} + v\frac{\partial u}{\partial y} = U\frac{\mathrm{d}U}{\mathrm{d}x} + \frac{\partial^2 u}{\partial y^2} \quad (14)$$

$$u\frac{\partial\theta}{\partial x} + v\frac{\partial\theta}{\partial y} = \frac{1}{Pr}\frac{\partial^2\theta}{\partial y^2} \quad (15)$$

and the boundary conditions for water flowing on an ice surface are

$$\text{at } y = 0 \; u = 0; \; v = v_0; \; \theta = 0$$
$$\text{at } y = \delta_u \; \frac{\partial u}{\partial y} = 0; \; \frac{\partial^2 u}{\partial y^2} = 0; \; u = U(x) \quad (16)$$
$$\text{at } y = \delta_t \; \frac{\partial \theta}{\partial y} = 0; \; \frac{\partial^2 \theta}{\partial y^2} = 0; \; \theta = 1.$$

Another boundary condition at the melting interface is realized by considering an energy balance across the interface.

$$\text{at } y = 0 \quad v_0 = \frac{Ste}{Pr} \frac{\partial \theta}{\partial y}\bigg|_{y=0}. \quad (17)$$

Note that equation (17) assumes that no heat is conducted to the melting interface from the solid phase.

In non-dimensionalizing these equations and boundary conditions the following non-dimensionalizations are employed. Distances and velocities along the surface are non-dimensionalized with respect to the jet diameter or jet slot width and incoming jet velocity respectively. Distances and velocities normal to the surface are non-dimensionalized with respect to the jet diameter or jet slot width and incoming jet velocity along with the square root of Reynolds number based on the incoming jet velocity and the jet diameter or slot width. For example, $y = (\bar{y}/D)\sqrt{Re_D}$; $v = (\bar{v}/V)\sqrt{Re_D}$ where $\bar{y}$ and $\bar{v}$ are the dimensional quantities. The non-dimensional temperature is defined by $\theta = (T - T_0)/(T_\infty - T_0)$ where T_∞ is the jet bulk temperature and T_0 is the melting surface temperature 0°C. The Stefan number, *Ste*, gives the ratio of the specific heat of the fluid to the latent heat required for the melting process and is given by $Ste = C_p(T_\infty - T_0)/q_L$ where q_L is the latent heat of fusion.

Equations (13), (14) and (15) with boundary conditions (16) and (17) were solved using the von Karman–Pohlhausen integral method with a fourth order polynomial representing the velocity and temperature distributions. Integration of the continuity equation (13) from $y = 0$ to $y = \delta$ results in

$$v_\delta = v_0 - \frac{1}{r^n} \int_0^\delta \frac{\partial}{\partial x}(r^n u)\,dy. \quad (18)$$

Integrating the momentum equation (14) from $y = 0$ to $y = \delta_u$, utilizing equation (18) and boundary conditions (16) one obtains [10]

$$\frac{U}{r^n}\frac{d}{dx}(r^n\delta_2) + \delta_2\frac{dU}{dx}\left(2 + \frac{\delta_1}{\delta_2}\right) = \frac{1}{U}\frac{\partial u}{\partial y}\bigg|_{y=0} + \frac{Ste}{Pr}\frac{\partial \theta}{\partial y}\bigg|_{y=0} \quad (19)$$

where δ_1 and δ_2 are the displacement thickness and momentum thickness defined by

$$\delta_1 = \int_0^{\delta u}\left(1 - \frac{u}{U}\right)dy$$
$$\delta_2 = \int_0^{\delta u}\frac{u}{U}\left(1 - \frac{u}{U}\right)dy. \quad (20)$$

Similarly, the energy equation is integrated from $y = 0$ to $y = \delta_t$ and the result is

$$\frac{U}{r^n}\frac{d}{dx}(r^n\delta_3) + \delta_3\frac{dU}{dx} = \left(\frac{1 + Ste}{Pr}\right)\frac{\partial \theta}{\partial y}\bigg|_{y=0} \quad (21)$$

where δ_3 is an energy thickness defined by

$$\delta_3 = \int_0^{\delta_t}\frac{u}{U}(1 - \theta)\,dy. \quad (22)$$

One can see that the momentum equation (19) and the energy equation (21) are coupled through the melting condition at the interfacial boundary, equation (17). The fourth order polynomial used to represent the velocity distribution in the boundary layer is

$$\frac{u}{U} = \frac{1}{1 + \lambda_0'}\left\{2\eta_1 - 2\eta_1^3 + \eta_1^4 + \lambda_0'(6\eta_1^2 - 8\eta_1^3 + 3\eta_1^4) + \frac{\Lambda}{6}(\eta_1 - 3\eta_1^2 + 3\eta_1^3 - \eta_1^4)\right\} \quad (23)$$

where $\eta_1 = y/\delta_u$; λ_0' is a melting parameter defined by $\lambda_0' = v_0\delta_u/6$ and Λ is a pressure gradient parameter defined by $\Lambda = \delta_u^2(dU/dx)$. The coefficients for this velocity profile were evaluated by applying the boundary conditions (16) and the momentum equation (14) evaluated at $y = 0$ to a general expression for a fourth order polynomial. Equation (23) reduces to the one presented in [3] when the pressure gradient is zero, that is $\Lambda = 0$. For the case of no melting, $\lambda_0' = 0$ and equation (23) reduces to profile presented in [10].

With a similar procedure one obtains the fourth order polynomial temperature distribution.

$$\theta = \frac{1}{(1 + \lambda_0 Pr)}\left\{(2\eta - 2\eta^3 + \eta^4) + \lambda_0 Pr(6\eta^2 - 8\eta^3 + 3\eta^4)\right\} \quad (24)$$

where λ_0 is a melting parameter defined by $\lambda_0 = v_0\delta_t/6$ and $\eta = y/\delta_t$. The coefficients of the temperature profile were evaluated by applying boundary conditions (16) and the energy equation (15) evaluated at $y = 0$ to a general expression for a fourth order polynomial.

The quantities $(1/U)(\partial u/\partial y)|_{y=0}$ and $(\partial\theta/\partial y)|_{y=0}$ which represent the shear stress coefficient and the heat-transfer rate may now be found using equations (23) and (24).

$$\frac{1}{U}\frac{\partial u}{\partial y}\bigg|_{y=0} = \frac{1}{\delta_u}\left(\frac{2 + (\Lambda/6)}{1 + \lambda_0'}\right) \quad (25)$$

$$\frac{\partial \theta}{\partial y}\bigg|_{y=0} = \frac{1}{\delta_t}\left(\frac{2}{1 + \lambda_0 Pr}\right). \quad (26)$$

The solution procedure for the momentum equation is similar to that outlined in Schlichting [10]. Multiplying the momentum equation (19) by δ_2 and using equations (25) and (26) one obtains

$$\frac{u}{2}\frac{d\delta_2^2}{dx} + \frac{U\delta_2^2}{r^n}\frac{dr^n}{dx} + \delta_2^2\frac{dU}{dx}\left(2 + \frac{\Delta_1}{\Delta_2}\right) = \Delta_2\left\{\frac{2 + (\Lambda/6)}{1 + \lambda_0'} + \frac{2Ste}{Pr(1 + \lambda_0 Pr)m}\right\} \quad (27)$$

where

$$\Delta_1 = \frac{\delta_1}{\delta_u} = \int_0^1 \left(1 - \frac{u}{U}\right) d\eta_1$$
$$\Delta_2 = \frac{\delta_2}{\delta_u} = \int_0^1 \left(1 - \frac{u}{U}\right)\frac{u}{U} d\eta_1. \quad (28)$$

The ratio of boundary-layer thicknesses

$$m = \delta_t/\delta_u \quad (29)$$

in the momentum equation (27) produces the coupling between this equation and the energy equation.

With the velocity distribution of equation (23), the thicknesses Δ_1 and Δ_2 in equation (28) may be found directly. Performing the required integrations,

$$\Delta_1 = \frac{1}{1+\lambda_0'}\left\{\frac{3}{10} - \frac{\Lambda}{120} + \frac{2\lambda_0'}{5}\right\} \quad (30)$$

$$\Delta_2 = \frac{1}{63(1+\lambda_0')^2} \times\left\{\frac{37}{5} - \frac{\Lambda}{15} - \frac{\Lambda^2}{144} + \frac{\Lambda\lambda_0'}{10} + \frac{156\lambda_0'}{10} + \frac{36\lambda_0'^2}{5}\right\}.$$

These expressions reduce to those given in [10] for the case of no melting, that is when $\lambda_0' = 0$.

The integration of equation (27) is accomplished by introducing the quantities

$$Z = \delta_2^2 \quad (31)$$

$$K = \delta_2^2 \frac{dU}{dx} = Z\frac{dU}{dx}. \quad (32)$$

The parameter K is a known function of the pressure gradient parameter Λ;

$$K = \frac{\delta_2^2}{\delta_u^2}\delta_u^2\frac{dU}{dx} = \Delta_2^2\Lambda. \quad (33)$$

The integral momentum equation (27) now becomes

$$\frac{dZ}{dx} = \frac{2}{U}\left\{\Delta_2\left(\frac{2+(\Lambda/6)}{1+\lambda_0'} + \frac{2Ste}{Pr(1+\lambda_0 Pr)m}\right) - \frac{U}{r^n}\frac{K}{dU/dx}\frac{dr^n}{dx} - K\left(2 + \frac{\Delta_1}{\Delta_2}\right)\right\}. \quad (34)$$

Introduce the transformation

$$Z^* = (r^n)^2 Z \quad (35)$$

equation (34) becomes

$$\frac{dZ^*}{dx} = \frac{2(r^n)^2}{U}\left\{\Delta_2\left(\frac{2+(\Lambda/6)}{1+\lambda_0'} + \frac{2Ste}{Pr(1+\lambda_0 Pr)m}\right) - K\left(2 + \frac{\Delta_1}{\Delta_2}\right)\right\}. \quad (36)$$

The melting parameters λ_0' and λ_0 are related to the Stefan number and the ratio of boundary-layer thicknesses, m. From the definitions of the melting parameters, $\lambda_0 = m\lambda_0'$ and using equations (17) and (26)

$$Ste = 3\lambda_0 Pr(1+\lambda_0 Pr). \quad (37)$$

The transformations for the energy equation are very similar to those for the momentum equation. Introduce

$$W = \delta_3^2 \quad (38)$$

$$L = \delta_3^2\frac{dU}{dx} \quad (39)$$

and the integral energy equation becomes

$$\frac{dW}{dx} = \frac{2}{U}\left\{\Delta_3\left(\frac{2}{Pr(1+\lambda_0 Pr)} + 6\lambda_0\right) - L - \frac{L}{r^n}\frac{U}{dU/dx}\frac{dr^n}{dx}\right\} \quad (40)$$

where Δ_3 is an energy thickness defined by

$$\Delta_3 = \frac{\delta_3}{\delta_t} = \int_0^1 \frac{u}{U}(1-\theta)\,d\eta. \quad (41)$$

With the velocity distribution (23) and temperature distribution (24) the thickness Δ_3 may be found explicitly. Performing the required integrations one obtains

$$\Delta_3 = \frac{1}{(1+\lambda_0 Pr)(1+\lambda_0')} \times\{C_1(m) + \Lambda C_2(m) + \lambda_0' C_3(m) + \lambda_0 Pr C_4(m) + \lambda_0 Pr\Lambda C_5(m) + \lambda_0 Pr\lambda_0' C_6(m)\} \quad (42)$$

where

$$C_1(m) = \frac{2m}{15} - \frac{3m^3}{140} + \frac{m^4}{180}$$
$$C_2(m) = \frac{m}{90} - \frac{m^2}{84} + \frac{9m^3}{1680} - \frac{65m^4}{216}$$
$$C_3(m) = \frac{m^2}{14} - \frac{3m^3}{35} + \frac{m^4}{60}$$
$$C_4(m) = \frac{m}{5} - \frac{m^3}{14} + \frac{m^4}{105} \quad (43)$$
$$C_5(m) = \frac{m}{60} - \frac{2m^2}{105} + \frac{m^3}{112} - \frac{m^4}{630}$$
$$C_6(m) = \frac{8m^2}{35} - \frac{m^3}{7} + \frac{m^4}{35}.$$

Again introducing a substitution similar to equation (35)

$$W^* = (r^n)^2 W \quad (44)$$

and equation (40) becomes

$$\frac{dW^*}{dx} = \frac{2(r^n)^2}{U}\left\{\Delta_3\left(\frac{2}{Pr(1+\lambda_0 Pr)} + 6\lambda_0\right) - L\right\}. \quad (45)$$

Equations (36) and (45) were solved using a Runge–Kutta integration technique. To start the integration procedure, however, stagnation point values of the pressure gradient parameter Λ and the boundary-layer thickness ratio m must be found. At the stagnation point the mainstream velocity is zero and equations (34) and (40) exhibit a singularity at this point. Because of the finite nature of δ_2 and δ_3 in the

region of the stagnation point, the quantities in brackets on the RHS of equations (34) and (40) must be zero at the stagnation point. Furthermore, for the two-dimensional planar case, $n = 0$, the term containing dr^n/dx vanishes and for the axisymmetric case, $n = 1$, the assumption that

$$\lim_{x \to 0} \frac{U}{\dfrac{dU}{dx}} \frac{\dfrac{dr^n}{dx}}{r^n} = 1$$

can be made [10]. The stagnation conditions therefore become

$$\Delta_2\left(\frac{2+(\Lambda/6)}{1+\lambda_0'} + 6\lambda_0'\right) - nK - K\left(2 + \frac{\Delta_1}{\Delta_2}\right) = 0$$
$$\Delta_3\left(\frac{2}{Pr(1+\lambda_0 Pr)} + 6\lambda_0\right) - (n+1)L = 0. \tag{46}$$

The simultaneous solution of these equations gives the pressure gradient parameter, Λ_0, and the boundary-layer thickness ratio, m_0, at the stagnation point.

In the integration of equations (36) and (45) the commonly used assumption of a constant ratio of boundary-layer thicknesses, m, was made. The value of m used was the value calculated at the stagnation point, m_0. With this assumption the momentum equation (36) can be integrated separately from the energy equation (45). Using the stagnation point values, Λ_0 and m_0, the value of Z at the next position downstream can be calculated. Knowing Z and obtaining dU/dz from the potential flow solution the value of K at the new position, say K_1, may be found from equation (32). The value of the pressure gradient parameter, Λ, at this position can then be found as the root of the equation

$$K(\Lambda) - K_1 = 0 \tag{47}$$

where $K(\Lambda)$ is the known explicit function of pressure gradient given by equation (33). The integration of the momentum equation in this manner gives Λ as a function of position along the impingement surface. Using the values of Λ, equation (45) can then be integrated to give W as a function of position. The thermal boundary-layer thickness is then given by

$$\delta_t = \sqrt{W}/\Delta_3.$$

This value in equation (26) gives the gradient of the non-dimensional temperature at the wall and thus the heat-transfer coefficient. Expressed in terms of a Nusselt number

$$\frac{Nu_D}{\sqrt{Re_D}} = \left.\frac{d\theta}{dy}\right|_{y=0} = \frac{\Delta_3}{\sqrt{W}}\left(\frac{2}{1+\lambda_0 Pr}\right). \tag{48}$$

From the integrations of equations (36) and (45) separate calculations of δ_u and δ_t were made. A test of the assumption of a constant ratio δ_u/δ_t can therefore be made. It was found that if the original constant value m_0 was replaced by this calculated ratio and the integrations were redone, only a very small change in the results occurred. Note that solution details concerning the finite element technique, the adjustment of the free surface and the integral boundary-layer calculations can be found in [11].

RESULTS

The problem of a two-dimensional jet impinging on a flat plate was used as a test problem for the solution technique just described. This problem was used because a number of other calculations exist with which the results can be compared. For the potential flow part of this problem an exact solution can be obtained using a conformal mapping of the flow field [12]. The distribution of velocity along the impingement surface for dimensionless nozzle plate spacings of $H = \infty$, 3.0, 1.0, 0.5 and 0.25 are shown in Fig. 2. Also

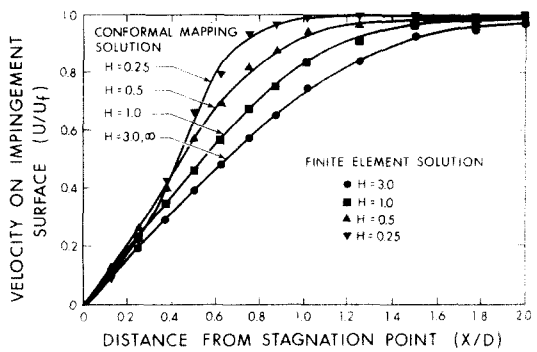

FIG. 2. Velocity distribution on a flat plate produced by the impingement of a two-dimensional free jet.

shown are the velocities predicted by the finite element method. For the finite element method the flow field was broken into 138 elements 329 nodes for all cases of nozzle-plate spacing used. In these calculations the case of $H = 0.25$ presents the most difficulty because of the rapid changes in velocity that occur near the nozzle lip. More nodes would be required in this region in order to obtain an accurate prediction of the velocity distribution. Accuracy of this prediction is particularly critical since a numerical differentiation of the velocity was performed. It was found that the velocity gradients obtained using the cubic spline numerical differentiation technique [13] were within 10% of the values calculated from the exact solution for all cases except the case of $H = 0.25$. For $H = 0.25$ errors in the velocity gradient of up to 18% existed near the nozzle lip.

To test the integral boundary-layer solution the distribution of the heat-transfer parameter $Nu_D/Re_D^{1/2}$ along the impingement surface was calculated. The results of the present calculations are shown in Fig. 3 along with two other calculations of the same parameter. First the value of this parameter can be estimated at the stagnation point using the similarity analysis of stagnation point flow of an infinite fluid [14]. This analysis, which assumes that the gradient of velocity is a constant known value, gives

$$Nu_D/Re_D^{1/2} = G(Pr)\left(\frac{dU}{dx}\right)_0^{1/2} \tag{49}$$

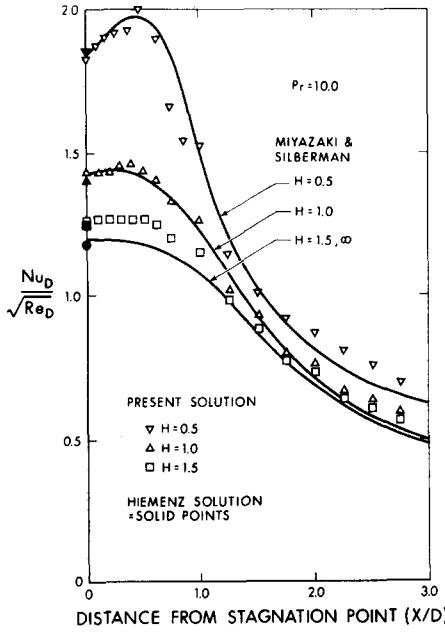

FIG. 3. Heat transfer on a flat plate produced by the impingement of a two-dimensional free jet.

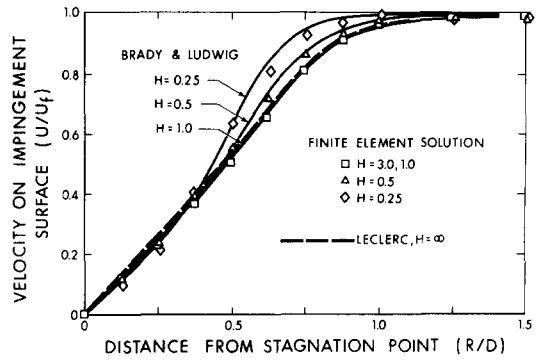

FIG. 4. Velocity distribution on a flat plate produced by the impingement of an axisymmetric free jet.

where $(dU/dx)_0$ is the freestream velocity gradient at the stagnation point. The function $G(Pr)$ has a value of 1.3388 for two-dimensional flow when $Pr = 10$ [15], the value of Prandtl number used in the two-dimensional problem. For the results shown in Fig. 3 the values of velocity gradient used in equation (49) were those calculated at the stagnation point from the conformal mapping solution. The results are within 3.5% of the present calculations of stagnation point heat transfer. Calculations of the distribution of heat transfer along the impingement surface have been made for this problem by Miyazaki and Silberman [16]. These calculations which used a finite difference procedure to calculate the boundary-layer growth are also shown in Fig. 3. The results from [16] and the present results show the same qualitative behavior. In particular, a peak in the heat transfer near the lip of the nozzle is predicted in both calculations. The peak is produced by a large gradient of velocity existing locally near the lip of the nozzle for small nozzle plate spacings in Fig. 2. Equation (49) suggests that the heat transfer is proportional to the square root of the gradient of velocity near the stagnation point. The quantitative agreement between the two results is fairly good except for the case of $H = 1.5$. This discrepancy may be explained as follows. Miyazaki and Silberman concluded that the case of $H = 1.5$ was equivalent to the case of $H = \infty$ [16]. However, if the velocity distribution for $H = \infty$ is used to calculate the heat transfer for the case of $H = 1.5$ an error of approximately 3% would occur in the results. The results of [16] adjusted by this amount (dotted line in Fig. 3) are in close agreement with the results of the present calculation for $H = 1.5$.

To further check the present solution method the case of an axisymmetric jet impinging on a flat plate was solved. The velocity distribution on the impingement surface predicted by the finite element method for nozzle-plate spacings of $H = 3.0$, 1.0 and 0.5 are shown in Fig. 4. Also shown are some experimental results. Brady and Ludwig [17] have measured the pressure distribution on the impingement surface and then calculated the velocity distribution from Bernoulli's equation. Leclerc [18] has used the electrical analogy to determine the potential flow field of the axisymmetric impinging jet. The finite element analysis used 144 elements with 343 nodes. The same arguments as to accuracy as discussed for the two-dimensional case apply to the case of axisymmetric jet impingement. It was found that nozzle-plate spacings of $H = 3.0$ and $H = 1.0$ were essentially the same and therefore $H = 1.0$ models the case of $H = \infty$. Note that in the case of $H = \infty$ for the axisymmetric jet the gradient of velocity exhibits a maximum near the lip of the nozzle. For $H = \infty$ in the two-dimensional case no maximum existed as shown in Fig. 2. Because of the maximum in the gradient of velocity a maximum is predicted in the heat transfer near the lip of the nozzle. The heat transfer as calculated from the integral boundary-layer technique for the axisymmetric jet impinging on a flat plate with nozzle-plate spacings of $H = 3.0$, 1.0 and 0.5 are shown in Fig. 5. As predicted a maximum in the heat-transfer curve exists near the lip of the nozzle. Also shown are the values at the stagnation point as given by equation (49). The value of $G(Pr)$ for axisymmetric flow and a Prandtl number of 13.7 is 1.3296 [15]. A Prandtl number of 13.7, the value for water at 0°C, was used so that these results could be compared with results where the effects of melting are included. The velocity gradient at the stagnation point was calculated from the finite element potential flow solution as no exact solution exists for the potential flow of axisymmetric jet impingement.

Next the problem of an axisymmetric jet impinging on a flat surface including the effect of melting was solved. The reference temperature for calculating the physical properties was chosen as the melting temperature 0°C. The solution technique was run for a range of Stefan numbers and the resulting heat-transfer curves are shown in Fig. 6. As the temperature of water is limited to the range $0°C \leqslant T_\infty \leqslant 100°C$ the Stefan number is limited to the range $0 \leqslant Ste \leqslant 1.25$. As can be seen from the figure a decrease of up to 50% in the

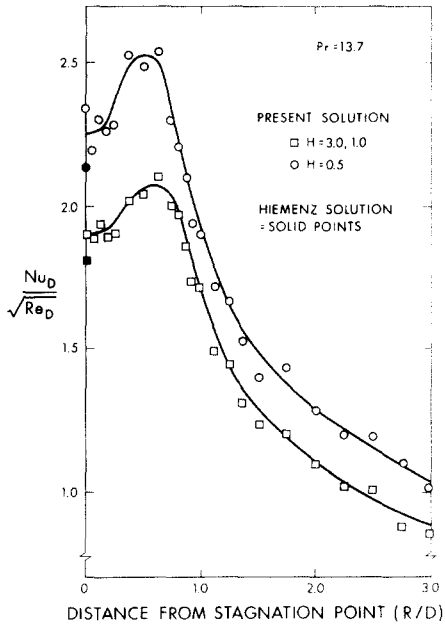

FIG. 5. Heat transfer on a flat plate produced by the impingement of an axisymmetric free jet.

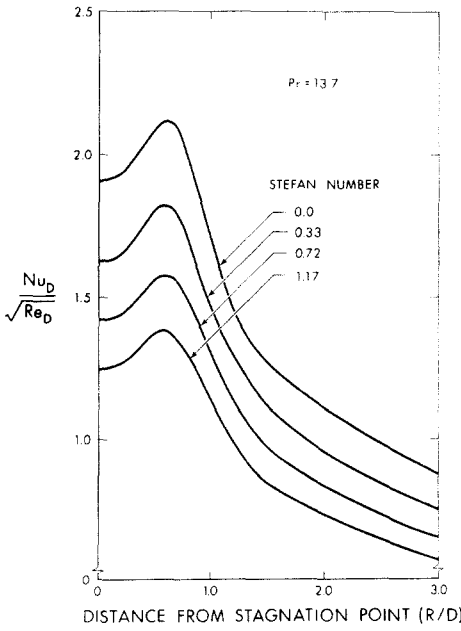

FIG. 6. The effect of melting on the heat transfer produced by an axisymmetric free jet impinging on a flat plate.

heat transfer exists for very large Stefan numbers. The decrease in heat transfer is caused by an increase in the amount of water being injected into the boundary layer due to the melting process. A thicker boundary layer decreases the temperature gradient at the melting ice surface and thus decreases the heat transfer according to equation (48). This behavior is similar to that calculated for flow over a flat plate [1–3].

CONCLUSIONS

The use of a finite element potential flow analysis combined with an integral boundary-layer analysis appears to be a fairly flexible computational technique for handling problems of jet impingement heat transfer. This technique produced good agreement with results of other techniques, where they were available, for both two-dimensional planar and axisymmetric jets. In general the technique could be used for any problem involving forced convection where distinct regions of potential flow and boundary-layer flow exist. A free surface or arbitrarily shaped solid surface can be handled with no difficulty by the finite element technique. The limitations are, however, that the flow be laminar and that no regions of separated flow exist.

One of the main numerical difficulties with this technique involves the matching of the solutions between the potential flow and the boundary-layer regions. The integral boundary-layer solution requires as an input the free stream velocity and its first derivative along the impingement surface. Since these parameters are calculated by a numerical differentiation of the finite element solution for the potential flow a high degree of accuracy and smoothness of these results are required. This factor was found to control the finite element nodal spacing required in regions of rapidly varying velocity.

In the boundary-layer model the effects of melting on the heat-transfer coefficients have been included. The case of heat transfer to a flat surface including the melting effect was solved. This is a somewhat unrealistic case; however, since the melting on the impingement surface is found to be non-uniform, the impingement surface would actually become distorted as melting proceeds. In principle the technique described in the paper could be made to handle this problem since the finite element and the integral boundary-layer solutions work equally well for a non-flat impingement surface. With appropriate modifications the technique therefore has the potential of analyzing a large class of problems involving phase change where the shape of the heat-transfer surface and the distribution of heat transfer on it are co-determined. An investigation of these problems is continuing.

REFERENCES

1. Y. C. Yen and C. Tien, Laminar heat transfer over a melting flat plate: the modified Levesque problem, *J. Geophys. Res.* **68**(12), 3673–3678 (1963).
2. F. M. Pozvonkov, E. F. Shurgalskii and L. S. Akselrod, Heat transfer at a melting flat surface under conditions of forced convection and laminar boundary layer, *Int. J. Heat Mass Transfer* **13**, 957–962 (1970).
3. O. M. Griffen, Heat, mass and momentum transfer during the melting of glacial ice in sea water, *J. Heat Transfer* **95**, 317–323 (1973).
4. R. R. Gilpin, The ablation of ice by a water jet, *Trans. Can. Soc. Mech. Engrs* **2**(2), 91–96 (1973–74).
5. Y. C. Yen and A. Zehnder, Melting heat transfer with water jet, *Int. J. Heat Mass Transfer* **16**, 219–223 (1973).
6. M. Mellor, Cutting ice with continuous jets, Second International Symposium on Jet Cutting Technology, Cambridge, pp. G565–G576, Paper G5, April (1974).
7. O. C. Zienkiewicz, *The Finite Element Method in Engineering Science*, Chapter 15, McGraw-Hill, London (1971).
8. T. Sarpkaya and G. Hiriart, Analysis of curved target-type thrust reversers, *AIAA Jl* **13**(2), 185–192 (1975).
9. S. T. K. Chan, Finite element analysis of irrotational

flows of an ideal fluid, Ph.D. Thesis, Dept. of Civil Engineering, University of California at Davis (1971).
10. H. Schlichting, *Boundary Layer Theory*, 6th edn, Chapter 10. McGraw-Hill, New York (1968).
11. A. W. Lipsett, Jet impingement heat transfer including effect of melting, M.Sc. Thesis, Department of Mechanical Engineering, University of Alberta, Edmonton, Alberta, Canada (1976).
12. J. H. Michell, On the theory of free streamline, *Phil. Trans. R. Soc.* **181A**, 389–431 (1890).
13. J. H. Ahlberg, E. N. Nielsen and J. L. Walsh, *The Theory of Splines and their Application*, Chapter 2. Academic Press, New York (1967).
14. E. M. Sparrow and L. Lee, Analysis of the flow field and impingement heat/mass transfer due to a non-uniform slot jet, *J. Heat Transfer* **97**, 191–197 (1975).
15. F. M. White, *Viscous Fluid Flow*, Chapter 3, pp. 172–184. McGraw-Hill, New York (1974).
16. H. Niyazaki and E. Silberman, Flow and heat transfer on a flat plate normal to a two-dimensional laminar jet issuing from a nozzle of finite height, *Int. J. Heat Mass Transfer* **15**, 2097–2107 (1972).
17. W. G. Brady and G. Ludwig, Theoretical and experimental studies of uniform impinging jets, *Am. Helicopter Soc. J.* **8**(2), 1–13 (1963).
18. A. Leclerc, Deviation d'un jet liquide par une plaque normal à son axe. Determination de la surface libre par analogie electrique, *Houille Blanche* **5**, 816 (1950).

TRANSFERT THERMIQUE POUR UN JET LAMINAIRE INCIDENT AVEC EFFET DE FUSION

Résumé—On étudie analytiquement le problème du transfert thermique pour un jet laminaire d'eau qui frappe une surface. Le jet est divisé en deux parties, une région d'écoulement potentiel et une région de couche limite. La solution du problème de lecoulement potentiel est obtenue par la méthode intégrale de Karman–Polhausen. Cette méthode d'étude des transferts thermiques de jets incidents est testée sur des écoulements bidimensionnels plans et axisymétriques. Les résultats présentés incluent les effets de fusion qui se produisent sur la surface d'impact.

DER WÄRMEÜBERGANG BEIM AUFTREFFEN LAMINARER STRAHLEN UNTER EINBEZIEHUNG VON SCHMELZEFFEKTEN

Zusammenfassung—Der Wärmeübergang beim Auftreffen laminarer Strahlen wird analytisch untersucht. Der Strahl wird in zwei Strömungsbereiche unterteilt, einen Potential- und einen Grenzschichtbereich. Die Potentialströmung wird mit Hilfe der Methode finiter Elemente gelöst. Für die Grenzschichtströmung wird die Karman–Pohlhausen–Integralmethode verwendet. Dieses Berechnungsverfahren für den Wärmeübergang auftreffender Strahlen wird anhand zweidimensionaler ebener und rotationssymmetrischer Strömungen getestet. Außerdem werden Ergebnisse angegeben für den Fall, daß an der Auftrefffläche ein Schmelzvorgang stattfindet.

ТЕПЛООБМЕН ПАДАЮЩЕЙ ЛАМИНАРНОЙ СТРУИ С УЧЕТОМ ОПЛАВЛЕНИЯ ПОВЕРХНОСТИ

Аннотация — Проведено аналитическое исследование процесса переноса тепла к поверхности от падающей на неё ламинарной водяной струи. Струйное течение разделено на две области: потенциального течения и течения в пограничном слое. Решение для потенциальной области получено методом конечных элементов, а для пограничного слоя — интегральным методом Кармана–Польгаузена. Предложенная методика решения проверена для двухмерных плоских и осесимметричных потоков. Также представлены результаты по оплавлению поверхности в точке падения струй.